AIChE

Damage Analysis of Microwave-Dried Materials

Stefan J. Kowalski, Jacek Banaszak, and Andrzej Rybicki
Dept. of Process Engineering, Poznań University of Technology, Institute of Technology and Chemical Engineering, pl. Marii Skłodowskiej Curie 2, 60-965 Poznań, Poland

DOI 10.1002/aic.12724
Published online July 25, 2011 in Wiley Online Library (wileyonlinelibrary.com).

The aim of this article is to analyze the drying-induced stresses and destruction of ceramic-like materials during their microwave drying. The kinetics of microwave drying at various microwave power levels are determined experimentally and numerically, and the distributions of temperature and moisture content in the tested samples are visualized with infrared camera and presented graphically. The experiments are performed on kaolin-clay samples, where destruction provoked by microwave drying is visualized on photographs taken with the photo camera and microscope. The thermo-hydro-mechanical model of drying elaborated by authors is used to determine the distribution of stress components and to calculate the effective stress required to induce the failure of material. The effective stress is formulated with the use of the energetic criterion, and the material spots prone to damage are predicted numerically. The numerically predicted spots are compared with the experimentally appointed places of material damage and a good adherence of the numerical predictions with experiments is confirmed. © 2011 American Institute of Chemical Engineers *AIChE J,* 58: 2097–2104, 2012
Keywords: microwave drying, damage, experiment, modeling, kinetics, stresses

Introduction

To improve the efficiency of the common convective drying, the microwave radiation is often used for the enhancement of this process in many materials,[1–3] among others, ceramic goods,[4–7] wood,[8,9] fruits, and vegetables,[10,11] pharmaceuticals,[12] and others. The advantages of microwave drying manifest themselves in a smaller energy consumption in comparison to the convective drying and a better quality of dried products, as far as it concerns their appearance and a mechanical state, or higher biological value in the case of food and medicine products. The overall time of drying is generally much shorter in microwave drying than in the purely convective one. All these positive effects may be gained, provided that the applied microwave power (MwP) is at an admissible level. Otherwise, the material may experience strong damage that could make the dried product useless.

Generally, the material exposed to microwave radiation is heated up to the boiling water temperature in the whole volume. Depending on dosed MwP, this process can proceed so intensively, that the rate of water evaporation inside the body is faster than the ability of water vapor efflux towards the material surface and further to the surroundings. As a result, one gets an overpressure within the body,[13,14] which causes material destruction inside the body, or even a kind of explosion in the extreme case. That is the reason why the samples after microwave drying do not reveal often cracks on their surface, but various kinds of damages are present inside the material. Wood, for example, can be burned inside during microwave drying with high MwP. One can also detect the big cavities inside the ceramic masses during microwave drying procured by a rapid increase of vapor pressure, etc. Thus, it is not sufficient to assess the quality of microwave-dried products by visual inspection of external surfaces.

The main aim of this article is to study the damage of clay-like materials and to analyze the quality of microwave-dried products at different MwP levels. Higher MwP involves faster drying, but unfortunately, it entails a risk of big deformations and material fractures that have a negative impact on the overall quality of final products.[15,16] The material fractures occur in stressed material due to complicated temperature and moisture content (MC) patterns with high temperature and MC gradients. To show this, the kinetics of drying is determined experimentally and numerically, and the distributions of temperature and MC are visualized with the use of infrared camera and are also numerically drawn up in graphs. The resulting thermal and hydro stresses generated due to the material expansion and contraction may cause cracks in the material when they exceed the failure strength of the material.

The damage and the development of crack formation in cylindrically shaped clay-like samples are visualized on photographs taken with the use of both photo camera and microscope. The spots of an enhanced risk to crack formation are determined numerically on the basis of thermo-hydro-mechanical drying model, elaborated earlier by authors. The effective stress and the energetic failure criterion of Huber-von Mises-Hencky is formulated to predict the spots of material-like damage.[17–19] The patterns of fractures arisen in the samples after microwave drying at four different MwPs are presented. A good adherence of the material spots prone to damage, predicted numerically with the places of real material damage determined experimentally is shown.

Correspondence concerning this article should be addressed to S. J. Kowalski at stefan.j.kowalski@put.poznan.pl.

© 2011 American Institute of Chemical Engineers

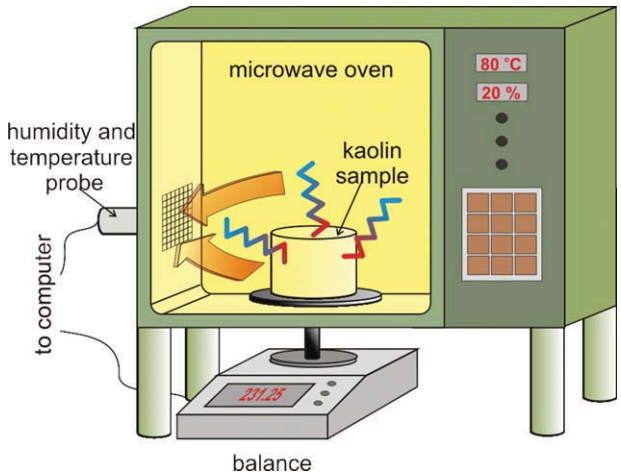

Figure 1. Outlook of the experimental setup.

[Color figure can be viewed in the online issue, which is available at wileyonlinelibrary.com.]

Experimental

KOC kaolin-clay from the Surmin-Kaolin SA Company, Nowogrodziec, Poland was the material investigated experimentally and theoretically in this article, and for this material some characteristic data necessary for numerical calculation of drying kinetics and drying-induced stresses are already given by the Surmin-Kaolin SA Company (see Table 1 in Kowalski et al.).[20] The KOC kaolin-clay is widely applied in ceramic industry for manufacturing sanitaryware and tableware. This kind of the material provides a good strength and plasticity during shaping of the mentioned products and reveals a reduced amount of pyroplastic deformation in the process of their firing.

The kaolin-clay delivered by the Surmin-Kaolin SA Company was in a dry state, and before experiments it was grinded and wetted with a predetermined amount of water and mixed to achieve a greasy paste of initial MC approximately equal to 0.45 kg water/kg dry kaolin. The greasy paste was stored and homogenized in a closed box for 48 h to unify moisture distribution in the whole material. The obtained soft kaolin-clay mass in such a way was used to mold cylindrical samples of diameter 0.06 m and height $h = 0.06$ m. The cylindrical samples were extruded from a special instrument to preserve their regular shape (Figure 4a), and samples of such a form were used for drying tests.

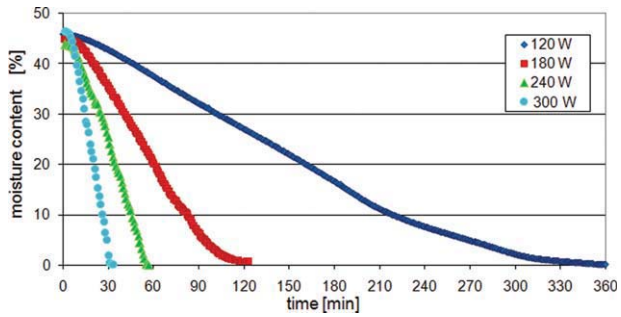

Figure 2. Drying curves of kaolin samples dried with different MwPs.

[Color figure can be viewed in the online issue, which is available at wileyonlinelibrary.com.]

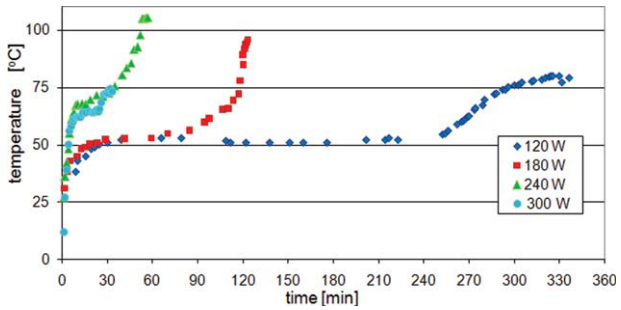

Figure 3. Temperatures measured at the sample upper surface.

[Color figure can be viewed in the online issue, which is available at wileyonlinelibrary.com.]

The cylindrical kaolin-clay samples were dried in the laboratory microwave dryer Plazmatronika WS 110 (Figure 1), and the working chamber has the dimensions: 300 × 400 × 450 mm^3 (height × width × depth). A distinct series of experiments were performed for the following magnetron output power levels: 120, 180, 240, and 300 W.

Figure 2 presents the drying curves obtained from experiments at the four mentioned MwPs. The drying curves at 120 and 180 W are characterized with the characteristic straight segments in the constant drying rated periods (CDRP) and nonlinear curves in the falling drying rate periods (FDRP). The other ones obtained with 240 and 300 W, in fact, do not expose explicit FDRP. The characteristic critical MC for kaolin-clay dried at 120 W MwP amounted to about 9–11%.

Figure 3 presents the surface temperatures of the samples measured with the pyrometer model MI produced by Raytek (precision 1°C), which is placed at the top corner of the microwave chamber dryer.

The pyrometer is a noncontacting instrument that intercepts and measures the thermal radiation emitted by the dried sample. The plots of the sample surface temperature show different durations of the CDRP more precisely than the drying curves presented in Figure 2 for different drying tests. The surface temperature becomes constant for 28 min at 300 W, for 42 min at 240 W, for 90 min at 180 W, and for 250 min at 120 W of MwP, respectively. The constant temperature at the sample surface was because of existence of water film on the surface and evaporation of water as from an open water surface. At the end of drying with 180 and 240 W MwP, the sample temperature rapidly rose up to 100°C despite the fact that the sample was almost dry. It means that dry kaolin also absorbs the microwave energy and warms itself. When drying with 300 W MwP the magnetron was switched off before reaching 100°C because a lot of microwave energy was reflected back to the magnetron.

The visual assessment of the sample surfaces after microwave drying indicates that, the samples dried with the lowest MwP of 120 W are of good quality and have no visible fractures or shape deformations (Figure 4a). The MwP of 120 W seems to be a proper one for kaolin drying. The samples subjected to 180 W MwP revealed different surface quality. Two samples of the four tested were of good quality, that is, without visible fractures at the surfaces and this looked like as shown in Figure 4a. The two others exposed noticeable fractures or even small chips coming off from the cylindrical samples (Figure 4b). Also, the bulgy shape deformations were observed on three samples.

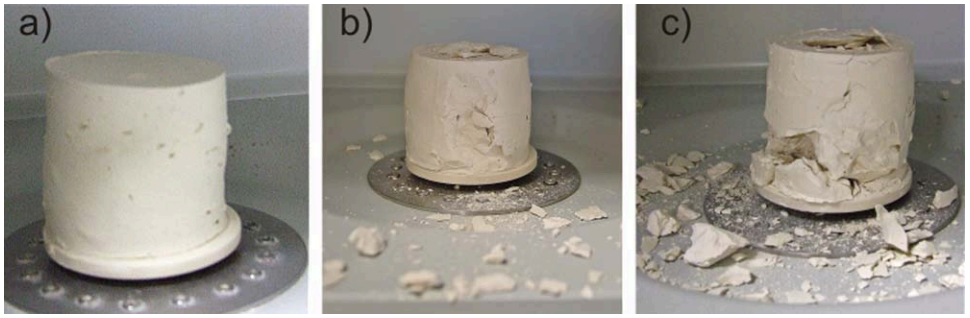

Figure 4. Samples during microwave drying with: (a) 120 W (no fractures), (b) 180 W (chips split off), and (c) 240 W (destroyed).

[Color figure can be viewed in the online issue, which is available at wileyonlinelibrary.com.]

The barrel shape was observed clearly on samples dried with 240 W MwP, and an explosion, which torn big pieces of the material, has appeared nearly at the end of drying process (Figure 4c). The fracture occurred mainly at the lower part and around of the cylindrical samples. Some split off kaolin pieces at the upper surface was observed for all higher MwP, similar as in the sample dried with 180 W MwP.

Figure 5 presents the photographs of the cylindrical samples after drying with 300 W MwP, and shows that the damage of the cylinder occurred around its center. This damage looks like an explosion caused by a high vapor pressure inside the cylinder because of intensive phase transitions of water into vapor. This justifies that by microwave heating the highest temperature arises inside the material, which is confirmed with IR camera picture presented in Figure 5c.

So, the samples subjected to 300 W MwP looked quite differently than those presented in Figure 4. These samples became a huge vertical slits, almost 3 cm long and 2.5 cm deep (Figure 5a). It was caused by the explosion already at the beginning of a drying process. The barrel shape of the samples is very clearly visible in both Figures 5a, b. The picture of temperature distribution in the longitudinal cross-section sample taken by the infrared camera (Flir thermacam B2) after 5 min of drying is presented in Figure 5c. The temperature reached about 90°C in some hot spots, although the mean temperature in the central part was about 72°C. This indicates the existence of places where the water was rapidly changed into vapor. The rapidly increased vapor pressure creates the big slit, so that the water vapor finds the way out.

Microscopic observations of the sample surfaces were carried out with the use of optical microscopy Zeiss Axiovert 25. The surface of the sample dried with 120 W MwP was generally without fractures, except of a single little scratch (Figure 6a) that is visible only in the microscopic zoom. Many fractures were noticed on sample surfaces dried with 180 and 240 W MwP (Figure 6b). They were much wider and longer than those in the previous case. Besides, in this case one could find a lot of little dry kaolin particles procured during fractures at the end of drying, when the material was almost dry.

The huge fractures in samples dried with 300 W MwP confirm the genesis on their explosive creation (Figure 6c). The fractures are very wide and are with irregular and rugged edges. The kaolin material during explosion was still wet and got a significant deformation.

Figure 7 presents the internal views of samples dried with 240 W MwP after 10 and 50 min of drying. It is visible that after 10 min of drying some fractures in central parts of the sample have appeared (Figure 7a). After 60 min of drying there were more visible fractures and also the internal structure of the sample became very incoherent (Figure 7b). This rough structure was procured by rapid evaporation of water inside the sample that induced a high pressure. Such a disheveled and nonuniform structure was also visible in some samples dried with 180 and 300 W MwP. The temperature inside the material was very high (nearly 80°C) in these two cases. The distributions of temperature were typical for microwave drying: higher temperature inside and the lower one close the surface. The real temperatures were even higher, however, the execution of the sample cross-section for temperature measurement took about 40 s, and during this time the sample lost some heat.

The view of samples dried with different MwPs is presented in Figure 8. As it is seen in Figure 8, only the sample

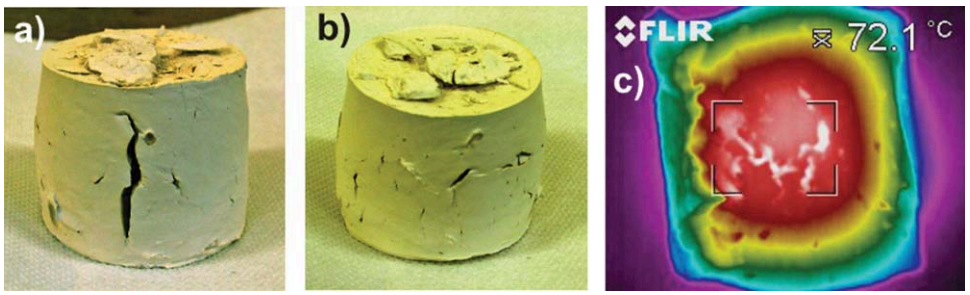

Figure 5. Kaolin sample subjected to 300 W MwP. (a) Front view, (b) rear view, and (c) IR camera picture of temperature distribution in the sample longitudinal cross-section after 5 min of drying.

[Color figure can be viewed in the online issue, which is available at wileyonlinelibrary.com.]

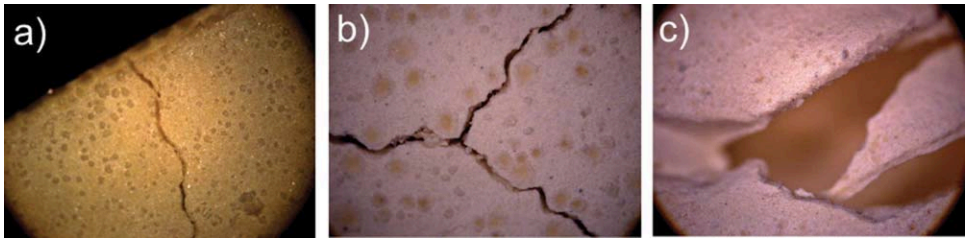

Figure 6. Kaolin samples dried with different MwP levels: (a) 120 W, (b) 180 W and 240 W, and (c) 300 W.

[Color figure can be viewed in the online issue, which is available at wileyonlinelibrary.com.]

dried with 120 W MwP has acceptable quality, that is, without visible cracks, flaws, interstices, etc. From the four samples dried with 180 W MwP two of them got a number of debris split off from the main body, and the two others did not fractured at all becoming only a slight barrel shape. The samples dried with 240 W MwP look fractured totally. They got a bulgy shape with lots of part split off, mainly from the lower part of the cylindrical sample, but also from the upper surface.

There is one huge vertical slit and some split parts at the upper surface in the sample, which was dried with 300 W MwP. This vertical slit occurs always at the initial stage of heating with 300 W MwP. Heating at 300 W causes very intensive phase transition of water into vapor and generates high pore pressure in the sample core. The kaolin-clay at this stage is not dry but still elastic–plastic. Therefore, there is no burst but a kind of blow up caused by the internal high pressure vapor. The deep crack is a result of the vapor efflux at high pressure. Such a phenomenon was repeated each time when the sample was heated at 300 W.

Modeling

The distribution of drying-induced stresses and the elastic energy accumulated in the material as well as the effective stress responsible for material failure are calculated for a kaolin-clay cylinder (Figure 9) subjected to microwave drying.

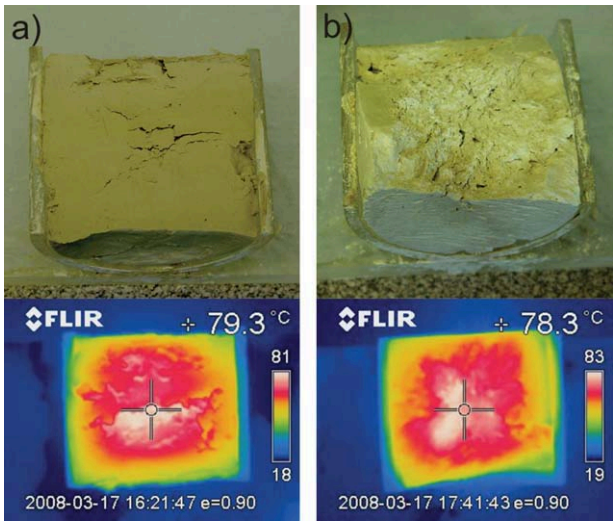

Figure 7. Cross-sectional view and IR view of samples dried with 240 W MwP after: (a) 10 min drying and (b) 60 min drying.

[Color figure can be viewed in the online issue, which is available at wileyonlinelibrary.com.]

The thermo-hydro-mechanical model of drying, which was used in this article for description of drying kinetics and determination of the state of stress during microwave drying is presented in Kowalski[21] and Kowalski and Rybicki.[22] We adopt this model to describe the stress state in the cylindrical sample. The description of cylinder deformation, expressed by the radial and longitudinal displacements u_r and u_z, is provided by the two coupled equations of the form.[22]

$$M\nabla^2 u_r + \frac{\partial}{\partial r}[(M+A)\varepsilon - \gamma_T\vartheta - \gamma_X\theta] = M\frac{u_r}{r^2} \tag{1}$$

$$M\nabla^2 u_z + \frac{\partial}{\partial z}[(M+A)\varepsilon - \gamma_T\vartheta - \gamma_X\theta] = 0 \tag{2}$$

where M and A denote the shear and bulk elastic modules, $\gamma_T = (2M + 3A)\kappa_T$, $\gamma_X = (2M + 3A)\kappa_X$ are the thermo and hydro modules with κ_T and κ_X representing the coefficients of linear thermal- and hydro-expansion, θ and ϑ denote the departure of liquid content and temperature from the reference state. In these equations

$$\nabla^2 = \frac{\partial^2}{\partial r^2} + \frac{1}{r}\frac{\partial}{\partial r} + \frac{\partial^2}{\partial z^2} \quad \text{and} \quad \varepsilon = \frac{\partial u_r}{\partial r} + \frac{u_r}{r} + \frac{\partial u_z}{\partial z} \tag{3}$$

denote the Laplace's operator for cylindrical geometry and the volumetric strain, respectively.

The mechanical boundary conditions express zero valued radial σ_{rr} and longitudinal σ_{zz} stresses on the external surfaces, and zero valued radial u_r and longitudinal displacements u_z on the cylinder axis and at the bottom surface of the cylinder, that is,

$$\sigma_{rr}|_{r=R} = \left[2M\frac{\partial u_r}{\partial r} + A\varepsilon - \gamma_T\vartheta - \gamma_X\theta\right]\Big|_{r=R.} = 0 \tag{4}$$

$$\sigma_{zz}|_{z=H} = \left[2M\frac{\partial u_z}{\partial z} + A\varepsilon - \gamma_T\vartheta - \gamma_X\theta\right]\Big|_{z=H.} = 0 \tag{5}$$

Figure 8. Kaolin samples dried with different MwP levels.

[Color figure can be viewed in the online issue, which is available at wileyonlinelibrary.com.]

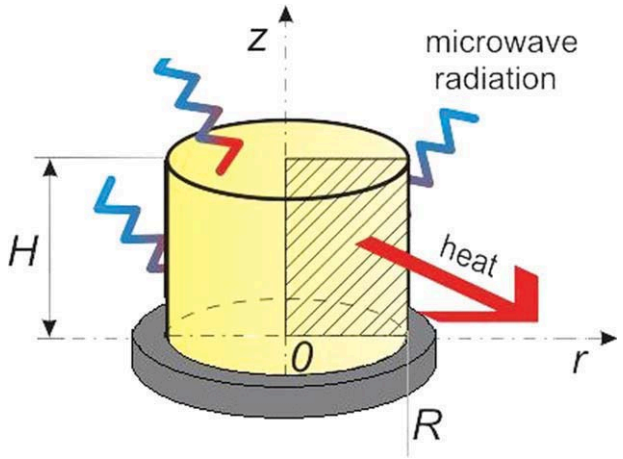

Figure 9. Geometry of cylindrical sample subjected to microwave drying.

[Color figure can be viewed in the online issue, which is available at wileyonlinelibrary.com.]

$$u_r|_{r=0} = 0 \quad \text{and} \quad u_z|_{z=0} = 0 \tag{6}$$

Having determined the displacements and strains one can calculate stresses using the suitable physical relations.[23] The state of stress in the cylinder is fully described by four components of the stress tensor, namely: radial σ_{rr}, circumferential $\sigma_{\varphi\varphi}$, longitudinal σ_{zz}, and shear σ_{rz} stresses, with $\sigma_{r\varphi}=0$, $\sigma_{z\varphi} = 0$. The stress components σ_{rr} and σ_{zz} are exposed by Eqs 4 and 5 and the components $\sigma_{\varphi\varphi}$ and σ_{rz} are formulated as follows

$$\sigma_{\varphi\varphi} = 2M\frac{u_r}{r} + A\varepsilon - \gamma_T\vartheta - \gamma_X\theta \quad \text{and} \quad \sigma_{rz} = 2M\left(\frac{\partial u_r}{\partial z} + \frac{\partial u_z}{\partial r}\right) \tag{7}$$

The effective stress is defined from the Huber-von Mises-Hencky energy hypothesis as:[22]

$$\sigma_{\text{eff}} = \frac{1}{2}\sqrt{(\sigma_{rr}-\sigma_{zz})^2 + (\sigma_{rr}-\sigma_{\varphi\varphi})^2 + (\sigma_{\varphi\varphi}-\sigma_{zz})^2 + 6\sigma_{rz}^2} \tag{8}$$

The material failure can take place if the effective stress exceeds the admissible one, which expresses the yield stress or the strength of the material at a given MC. The admissible stress was determined experimentally by Musielak[24,25] for kaolin-clay at different MCs. The experimental data for admissible stress have been interpolated by the following function

$$\sigma_{\text{adm}} = \sigma_0 + \sigma_X \exp(-C_\sigma\theta) \tag{9}$$

where $\sigma_0 = 142\,858$ Pa, $\sigma_X = 1\,688\,320$ Pa, and $C_\sigma = 29.6534$.

The failure of the material may happen if it becomes plastic or if the material strength will be violated in those regions of dried kaolin-clay cylinder in which

$$\sigma_{\text{eff}} \geq \sigma_{\text{adm}} \tag{9}$$

The distribution and time evolution of the MC in the kaolin-clay cylinder during drying is determined on the basis of differential equation of the form.[20,22]

$$\rho^s\dot{\theta} = \Lambda\left(\frac{\partial^2}{\partial r^2} + \frac{1}{r}\frac{\partial}{\partial r} + \frac{\partial^2}{\partial z^2}\right)(c_T\vartheta + c_X\theta) - \varpi(c_T\vartheta + c_X\theta), \tag{10}$$

The following boundary conditions describing the moisture exchange with the surrounding are applied

$$-\Lambda\nabla(c_T\vartheta + c_X\theta)|_{\partial B}\cdot\mathbf{n} = k_m(\mu^v|_{\partial B} - \mu_a) \text{ with } \nabla\theta\Big|_{\substack{r=0\\z=0}}\cdot\mathbf{n} = 0, \tag{11}$$

The initial condition expresses a uniform distribution of moisture at the beginning.

$$\theta(r,z,t)|_{t=0} = \theta_0 = \text{const} \tag{12}$$

In the above equations, Λ denotes the coefficient of moisture transfer, φ is the parameter responsible for the rate of phase transitions, c_T and c_X are the coefficients of moisture thermodiffusion and diffusion, k_m is the coefficient of convective vapor exchange between the dried body and the ambient air, $\mu^v|_{\partial B}$ and μ_a denote the chemical potentials of vapor in the air at the boundary surface and in the ambient air, respectively.

The chemical potentials for vapour in air can be expressed in terms of the molar ratio of the vapour content x[26]

$$\mu^v(p,T,x) = \mu^{\otimes}(p,T) + R^vT\ln x \tag{13}$$

where $\mu^{\otimes}$ is the chemical potential of pure vapor, R^v is the gas constant for vapor, p and T denote the air pressure and temperature.

Developing $\mu^{\otimes}$ into the Taylor series and leaving only the first term of this series we can write the difference between the chemical potentials of vapor in air at the boundary surface and in the ambient air as follows:

$$\mu^v|_{\partial B} - \mu_a = s^v(T|_{\partial B} - T_a) + R^v(T|_{\partial B}\ln x|_{\partial B} - T_a\ln x_a) \tag{14}$$

where s^v denotes the entropy of pure vapor per unit mass, $T|_{\partial B}$ and T_a are the temperatures, and $x|_{\partial B}$ and x_a are the molar ratios of vapor in air at the boundary surface and in the ambient air, respectively.

The spatial distribution and time evolution of the temperature is determined from the differential equation of the form.[21,22]

$$\dot{\vartheta} = \kappa\left(\frac{\partial^2}{\partial r^2} + \frac{1}{r}\frac{\partial}{\partial r} + \frac{\partial^2}{\partial z^2}\right)\vartheta - l\frac{\varpi}{\rho^s c_v}(c_T\vartheta + c_X\theta) + \Re \tag{15}$$

Equation 15 is supplemented with the following boundary and initial conditions.

$$\lambda\nabla\vartheta|_{\partial B}\cdot\mathbf{n} = k_T(\vartheta|_{\partial B} - \vartheta_a) - lk_m(\mu^v|_{\partial B} - \mu_a) \tag{16}$$

$$\nabla\vartheta|_{r=0} = 0, \quad \lambda\nabla\vartheta|_{z=0}\cdot\mathbf{n} = \bar{k}_T(\vartheta|_{z=0} - \vartheta_a), \quad \vartheta(r,z,t)|_{t=0} = \vartheta_0 = \text{const} \tag{17}$$

where $\lambda = (1-\phi)\lambda^s + \phi S\lambda^l$ is the heat conduction coefficient with λ^s and λ^l being the coefficients of heat conduction for skeleton and liquid, ϕ is the porosity, S is the pore saturation,

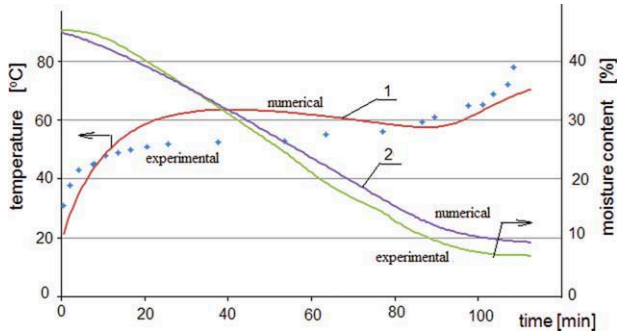

Figure 10. Drying kinetics at 120 W MwP: 1 – temperature at the sample surface, 2 – drying curve (overall humidity).

[Color figure can be viewed in the online issue, which is available at wileyonlinelibrary.com.]

k_T is the coefficient of convective heat exchange between the dried body and the ambient air at the free sample surfaces, $\bar{k}_T$ is the coefficient of convective heat exchange between the bottom sample surface resting on the metal plate and the ambient air, l is the latent heat of evaporation.

The radiation term $\Re$ in Eq. 15 describes the microwave heat source, and is formulated by the following formula[20]

$$\Re = \rho^s(a + b\theta)\exp(-2\delta L) \tag{18}$$

where δ is the parameter of decay of the microwave energy with distance L (here $\delta = 0$), and the coefficients $a = 126$ J/kg·s and $b = 20$ J/kg·s express the absorption of microwave energy by the skeleton and the moisture, respectively.

Results and discussion

The numerical calculations of moisture and temperature distributions and the state of stress in the cylindrical kaolin-clay sample were carried out for the following parameters[22]:

$H = 60$ mm,	$D = 60$ mm,
$c_T = 6.3{\cdot}10^2$ m^2/s^2 K,	$c_X = 1.11{\cdot}10^6$ m^2/s^2,
$\varphi = 2.5{\cdot}10^{-6}$ kg s/m^5,	$\kappa = 1.7{\cdot}10^{-3}$ m^2/s,
$k_m = 7.75\ 10^{-10}$ kg s/m^4,	$k_T = 12.5$ W/Km^2,
$c_v = 1.56{\cdot}10^{-2}$ J/kg·K,	$\rho^s = 2300$ kg/m^3,
$\lambda^s = 1.178$ W/m·K,	$\lambda^l = 0.597$ W/m·K,
$x_n = 0.75$,	$x_a = 0.075$,
$\theta_0 = 0.4$,	$T_a = 20$°C.

Figure 10 presents the drying kinetics curves determined numerically and experimentally for microwave drying at 120 W MwP.

We see that the drying model used in this article reflects very well both the drying curves and the temperature curves of the material determined experimentally. The good adherence of numerical and experimental results stimulates the hopes that the numerical results presented in this article are the proper ones.

Figure 11 illustrates the distribution of temperature in the half part of the cylindrical sample. Figure 11 shows the highest temperature generated around the center of the cylindrical sample, which is in accordance with the experimentally visualized distribution due to infrared camera measurement as presented in Figures 5c and 7.

Figure 12 illustrates the distribution of MC in the half part of the cylindrical sample. As it is visible in this figure the highest MC is at the bottom and in the center of the cylinder ($r = 0$, $z = 0$) and the lowest one is in the corner ($r = R$, $z = h$).

The distributions of several stress components are widely different. The stress components allow to calculate the overall effective stress, which maintains the failure of dried material. The effective and admissible stresses were computed on the basis of relations 8 and 9, respectively. Figure 13 presents spatial distributions of the overall effective stresses in the cross-section of a half cylinder shown in Figure 9. These stresses are computed as a functions of coordinates (r and z) at 60 min drying time by the application of 180 and 240 W MwP.

As it is seen in Figure 13, the greatest effective stress by drying at higher MwP (Figure 13a) arise at the cylinder surface around the bottom surface, that is, around the point (R,0), and also but of smaller value in some regions at the top part of the cylinder (R,H).

Figure 14 illustrates the regions in the half-cylinder where the effective stresses are greater than the admissible ones, that is, the regions where $(\sigma_{\text{adm}} - \sigma_{\text{eff}}) < 0$ for the two different MwP levels: 180 and 240 W. These regions are around point (R,0) and in the process with 240 W MwP also at the top of the sample (R,H). This figure shows the low relief map of possible material failure in the cylinder at 60 min drying time.

This prediction was confirmed experimentally by microwave drying of the kaolin cylinder in severe drying conditions by the application of 240 W, and in particular 300 W MwP (see Figures 5 and 8).

Figure 15 presents the time evolution of the effective stresses at different points of the cylinder by the application of 240 W MwP.

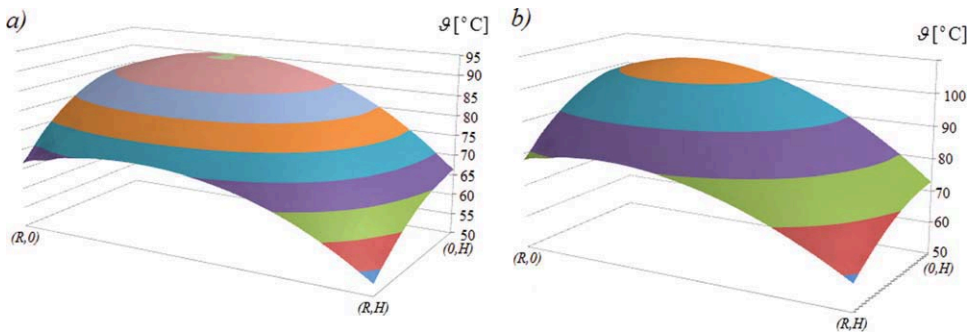

Figure 11. Temperature distribution in the half part of the cylindrical sample: (a) after 10 min drying and (b) after 60 min drying.

[Color figure can be viewed in the online issue, which is available at wileyonlinelibrary.com.]

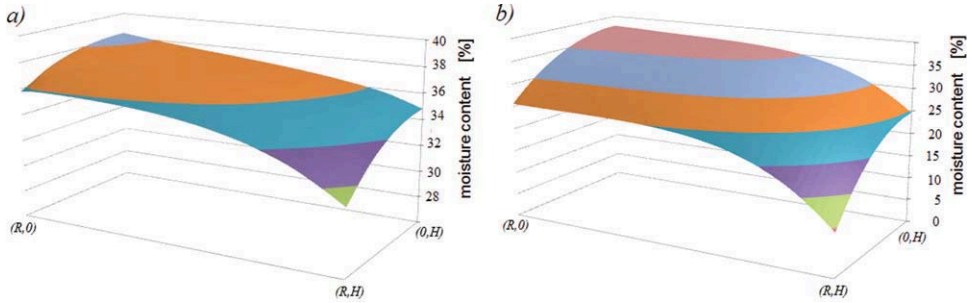

Figure 12. Distribution of MC in the half part of the cylindrical sample: (a) after 10 min drying and (b) after 60 min drying.

[Color figure can be viewed in the online issue, which is available at wileyonlinelibrary.com.]

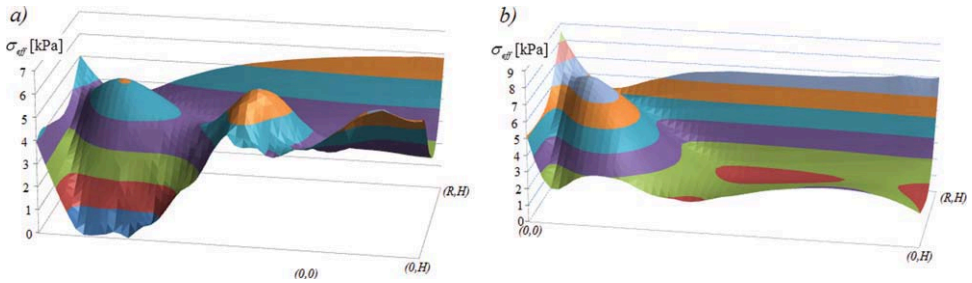

Figure 13. Distribution of effective stresses σ_{eff} in the longitudinal cross-section of the cylindrical half at 60 min drying time: (a) 180 W and (b) 240 W.

[Color figure can be viewed in the online issue, which is available at wileyonlinelibrary.com.]

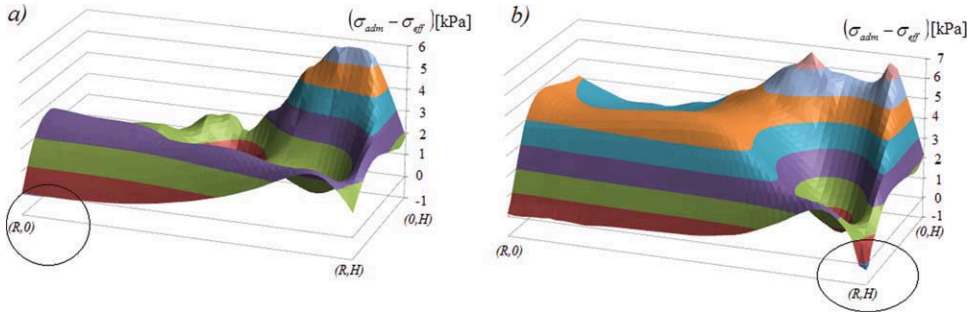

Figure 14. Regions in the cylinder cross section where ($\sigma_{adm} - \sigma_{eff}$) < 0 at 60 min drying time for the two different MwPs: (a) 180 W and (b) 240 W.

[Color figure can be viewed in the online issue, which is available at wileyonlinelibrary.com.]

This figure shows that the effective stress is zero at the beginning, then starts to increase attaining a maximum at some time (different for different points), and finally tends to zero at the final stage of drying. It is seen that the effective stress reaches maximum on the cylinder surface in the point (r = R, z = 0) at c.a. 60 min drying time.

Conclusions

MwP influences significantly the quality of dried kaolin samples. All samples dried with MwP above 120 W experienced damage. Samples dried with 180 W MwP are difficult for straightforward classification. All of them have incoherent internal structure after drying. Two of the four dried at this power level exhibited many fractures and split off pieces, but two others had no visible fractures at the external surfaces.

Many samples sustained bulgy deformation, which was associated with the intensive water evaporation and growth vapor pressure inside the material. Intensive evaporation caused a rapid increase of pore pressure, which resulted in disheveled and

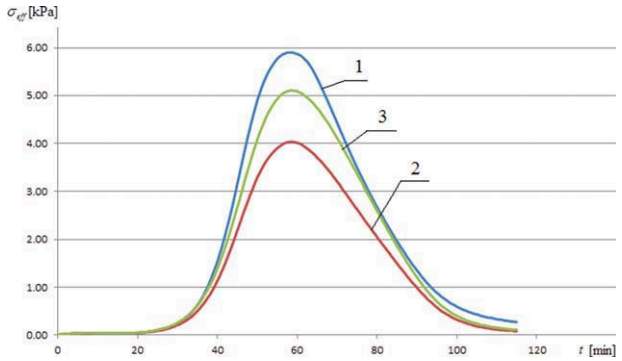

Figure 15. Time evolution of the effective stresses σ_{eff} at different points of the cylinder for 180 W MwP: 1 – point (*R*,0), 2 – point (0,*H*) and 3 – (*R*,*H*).

[Color figure can be viewed in the online issue, which is available at wileyonlinelibrary.com.]

incoherent structure of the material core. The samples at the beginning of drying still contains a lot of moisture and are very plastic and easy deformable. Sudden increase of vapor pressure inside these samples caused strong damage of explosive character, as it happened during drying with 300 W MwP (Figure 5a, and 8).

The drying-induced stresses can reach the material strength limit in some places of the dried samples. The thermo-hydro-mechanistic model of drying serves for a calculation of the drying stresses. Through comparison of the effective stress with the admissible stress the numerical analysis enables indication of the places, where the material damage can likely occur, as it is shown in Figure 14.

Acknowledgments

This work was carried out as a part of research project No N N209 104337 sponsored by Polish Ministry of Education and Science.

Notation

A, M = shear and bulk modules, MPa
c_T = thermodiffusion coefficient, $m^2\ s^{-2}\ K^{-1}$
c_X = diffusion coefficient, $m^2\ s^{-2}$
c_v = heat capacity, $J\ kg^{-1}\ K^{-1}$
H = sample height, m
k_m = mass convection coefficient, $kgsm^{-4}$
k_T = heat convection coefficient, $WK^{-1}\ m^{-2}$
l = latent heat of evaporation, $J\ kg^{-1}$
u_r, u_z = displacements, m
r, z = coordinates, m
R = sample radius, m
s = entropy, J/kg
t = time, s
T = temperature, K
x = molar ratio of vapor

Greek letters

δ = decay of microwave energy, m^{-1}
λ = heat transfer coefficient, $Wm^{-1}\ K^{-1}$
Λ = moisture transfer coefficient, $kg\ s\ m^{-3}$
ε = strain
κ_T = thermal linear expansion, K^{-1}
κ = humid linear expansion
μ = chemical potential, $J\ kg^{-1}$
ρ = mass density, $kg\ m^{-3}$
ϑ = temperature, °C
$\dot{\vartheta}$ = temperature time derivative, $°C\ s^{-1}$
θ = moisture content, $kg\ kg_{db}^{-1}$
$\dot{\theta}$ = moisture content time derivative, $kg\ kg_{db}^{-1}\ s^{-1}$
σ_{ij} = stress, kPa
φ = phase intensity coefficient, $kg\ s\ m^{-5}$
$\Re$ = microwave heat source, K^{-1}

Subscripts

a = ambient air
adm = admissible
eff = effective
m = moisture
r = radial
v = volume
T = thermal

Superscripts

s = solid
v = vapor

Literature Cited

1. Garcia H, Bueno JL. Improving energy efficiency in combined microwave-convective drying. *Drying Technol.* 1998;16:123–140.
2. Sanga ECM, Raghavan GSV, Mujumdar AS. *Heat and mass transfer during microwave-convection drying of composite materials: simulation with incorporation of shrinkage*. In: Mujumdar AS, editor, Proceedings IADC 2, Vera Cruz, Mexico, 2001:185–205.
3. Sanga ECM, Mujumdar AS, Raghavan GSV. Simulation of convection-microwave drying for shrinkage material. *Chem Eng Process.* 2002;41:487–499.
4. Segerer H. Producing technical ceramics by microwave drying, *Am Ceram Soc Bull.* 1998;77:64–66.
5. Feng H, Tang J, Cavalieri RP, Plumb OA Heat and mass transport in microwave drying of porous materials in a spouted bed. *AIChE J.* 2001;47:1499–1512.
6. Kowalski SJ, Rajewska K, Rybicki A. Mechanical effects in saturated capillary-porous materials during convective and microwave drying. *Drying Technol.* 2004;22:2291–2308.
7. Kowalski SJ, Rajewska K, Rybicki A. Stresses generated during convective and microwave drying. *Drying Technol.* 2005;23: 1875–1893.
8. Antti AL, Zhao H, Turner I. An investigation of the heating of wood in an industrial microwave applicator: theory and practice. *Drying Technol.* 2000;18:1665–1676.
9. Perre P, Turner IW. Microwave drying of softwood in an oversized waveguide. *AIChE J.* 1997;43:2579–2595.
10. Junge K, Tretau A. Microwave drying – not an alternative for the drying of shrink green products. *Ziegelindustrie Int.* 2005; 59:8–13.
11. Zhang M, Tang J, Mujumdar AS, Wang S. Trends in microwave related drying of fruits and vegetables. *Trends Food Sci Technol.* 2006;17:524–534.
12. Pakowski Z, Mujumdar AS. *Drying of pharmaceutical products.* In: Mujumdar AS, editor. *Handbook of Industrial Drying.* New York: Marcel Dekker, 1995:743–774.
13. Kowalski SJ, Rajewska K, Rybicki A. *Physical Fundamentals of Microwave Drying*. Poznań: Poznań University of Technology Publishers, 2005; (in Polish).
14. Itaya Y, Uchiyama S, Mori S. *Internal heating effect and enhancement of drying of ceramics by microwave heating with dynamic control*. In: Kowalski SJ, editor. *Drying of Porous Materials*. Dordrecht, The Netherlands: Springer, 2007:29–42.
15. Suhm J. Rapid wave microwave technology for drying sensitive products. *Am Ceram Soc Bull.* 2000;79:69–71.
16. Kowalski SJ, Rybicki A. Qualitative aspects of convective and microwave drying of saturated porous materials. *Drying Technol.* 2004;22:1173–1189.
17. Augier F, Coumans WJ, Hugget A, Kaasschieter EF. On the risk of cracking in clay drying. *Chem Eng J.* 2002;86:133–138.
18. Banaszak J, Kowalski SJ. Theoretical and experimental analysis of stresses and fractures in clay like materials during drying. *Chem Eng Process.* 2005;44:497–503.
19. Banaszak J, Kowalski SJ. Drying induced stresses estimated on the base of elastic and viscoelastic models. *Chem Eng J.* 2002; 86:139–143.
20. Kowalski SJ, Musielak G, Banaszak J. Heat and mass transfer during microwave-convective drying. *AIChE J.* 2010;56:24–35.
21. Kowalski SJ. *Continuous thermo-hydro-mechanical model using the theory of mixtures*. In:Tsotsas E,Mujumdar AS, editors. *Modern Drying Technology*. Weinheim: WILEY-VCH Verlag GmbH & Co. KGaA, 2007; 125–154.
22. Kowalski SJ, Rybicki A. Cohesive strength of materials during drying processes. *Drying Technol.* 2009;27:863–869.
23. Kowalski SJ. *Thermomechanics of Drying Processes*. Heilderberg-Berlin: Springer Verlag, 2003.
24. Musielak G. Possibility of clay damage during drying. *Drying Technol.* 2001;18:1645–1659.
25. Musielak G. *Modelling and Numerical Simulations of Transport Phenomena and Drying Stresses in Capillary-Porous Materials*. Poznań: Poznań University of Technology Publishers, 2004; (in Polish).
26. Szarawara J. *Chemical Thermodynamics*. Warszawa: WNT-Scientific Technological Publishers, 1985; (in Polish).

Manuscript received Mar. 21, 2011, and revision received May 13, 2011.